Lasers in Manufacturing Conference 2019

Ultrafast Laser Ablation at 1035 nm, 517 nm and 345 nm as a Function of Pulse Duration and Fluence

Norman Hodgson[a][*], Sebastian Heming[a], Albrecht Steinkopff[b], Hatim Haloui[b], Tony S. Lee[a]

[a]Coherent,Inc., 5100 Patrick Henry Drive, Santa Clara, CA 95054, USA
[b]Coherent Kaiserslautern GmbH, Opelstrasse 7, 67655 Kasierslautern, Germany

Abstract

Ablation rates for 25 materials (metals, semiconductors and dielectrics typically used in industrial manufacturing) were measured as a function of pulse duration (0.4 – 18 ps) and pulse fluence by using a 40 W modelocked, 1035 nm Yb Fiber MOPA operating at repetition rates of up to 1 MHz, with extra-cavity frequency doubling and frequency tripling. In addition to determining the maximum ablation rates and optimum pulse fluences, the heat affected zone and surface quality were analyzed. The data confirm the predictions by the two-temperature model. As long as the pulse fluence is close to the ~7.4 times the ablation threshold fluence, and the pulse duration is less than about 10 ps, the width of the heat affected zone is independent of pulse duration.

Keywords: Ultrafast laser ablation; ablation rate; femtosecond lasers; laser material processing; heat affected zone;

1. Introduction

The use of ultrafast lasers for industrial material processing has increased considerably in the last ten years due to the advent of medium-to-high power Nd and Yb-based amplifier systems with output powers of up to 100 W, pulse durations between 300 fs and 15 ps, and repetition rates of up to several MHz. The main advantage of using ultrafast pulses is the small heat affected zone (HAZ), combined with an increased energy penetration depth resulting from the high intensity of the laser pulse.

* Corresponding author. Tel.: +1-408-7646-09;
E-mail address: norman.hodgson@coherent.com .

For metals, HAZ of less than 5 µm can be achieved, while for plastic materials, the HAZ is typically in the range of 30 − 50 µm. Ablation rates can range from 0.2-0.3 mm^3/(W min) for metals and semiconductor materials to up to 5-10 mm^3/(W min) for absorbing dielectrics. Industrial ultrafast diode-pumped solid state and fiber MOPAs are now being used to cut foils for flat panel displays, to cut glass panels and sapphire substrates, to drill fuel injector nozzles, and for wafer scribing and surface micro-structuring. According to a recent market study by Strategies Unlimited, 2016, the global market for industrial applications for ultrafast lasers will be around 300 M$ in 2019, excluding ultrafast lasers being used in ophthalmic applications, which account for about 100 M$.

Very good progress has been made over the last decade to gain an understanding of the interaction between ultrashort pulses and the material, mostly based on the Two-Temperature Model initially used by Anisimov et al., 1974. This model connects light absorption by the electrons and the energy transfer to the lattice via a coupling term between the two systems with a characteristic transfer time, referred to as the electron-phonon relaxation time. Application of this model has provided a basic understanding of the ablation process, including the dependence of ablation threshold fluences, heat affected zones and ablation rates on the pulse duration (Sherman et al. 1989, Qiu et al., 1992, Nolte et al., 1997, Breitling et al., 2004). A more recent introduction of an ablation model by Neuenschwander et al., 2012, indicated that the ablation rate can be maximized by operating at an optimum pulse fluence of about 7.4 times the threshold fluence. In addition, it was discovered that the high speed of the ballistic electrons leads to an increase of the energy penetration depth as the pulse duration gets shorter (Neuenschwander et al., 2012, Wellershof et al., 1999).

While there have been many experimental studies to verify the validity of the Two-Temperature Model as well as the ultrafast ablation model, these investigations have been limited to the use of one laser wavelength and only for a limited number of materials. These publication mostly discuss ablation rates, while the main driving parameters for the use of ultrafast laser that are heat affected zone (HAZ) and surface quality have not been addressed in many publications, especially at laser wavelengths in the visible and ultraviolet.

In this paper, we report on the measurement of ablation rates, HAZ, and surface quality for 25 materials that are commonly used in industrial manufacturing, using laser wavelengths of 135 nm, 517 nm and 345 nm, and varying both the pulse duration and the pulse fluence. The result of this parametric study provides material-dependent guidelines for the optimization of the ultrafast ablation process and directions for the future development of ultrafast lasers.

2. Theoretical Description of Ultrafast Laser Ablation

For materials that exhibit free electrons, such as metals and semiconductors, the interaction of the ultrafast pulse with the material can be described by the Two-Temperature Models, which describes the temporal and spatial change in electron and lattice temperature, assuming absorption of the light energy by the electrons and transfer of the energy to the lattice with the electron-phonon relaxation time. The two coupled differential equations for electron temperature T_e and lattice temperature T_l read:

$$\frac{\partial T_e}{\partial t} = \frac{1}{C_e} \nabla(K_e \nabla T_e) - \frac{1}{\tau}(T_e - T_l) + \frac{\alpha}{C_e} A\, I(t) e^{-2r^2/w^2}\, e^{-\alpha z} \qquad (1)$$

$$\frac{\partial T_l}{\partial t} = \frac{1}{C_l} \nabla(K_l \nabla T_l) + \frac{1}{\tau}\frac{C_e}{C_l}(T_e - T_l) \qquad (2)$$

where C_e, C_l and K_e, K_l are the heat capacities and thermal conductivities of electron gas and lattice, respectively. The electron-phonon relaxation time τ (e-p relaxation time) generally increases with the

electron gas temperature with typical values at room temperature of less than 1 ps. Since heat conduction is mostly generated by electron movement, materials with higher thermal conductivity also exhibit longer e-p relaxation times. Copper, for instance, has an e-p relaxation time of about 800 fs at room temperature, while the corresponding value for Titanium is below 100 fs.

In general, the heat capacity of the electron gas is about 100 times lower compared to the lattice, which results in a 100x slower increase in the lattice temperature as compared to the electron temperature. While the light absorption and subsequent thermalization of the electrons occur on a timescale of about 100 fs, it may take the lattice tens of picoseconds to reach melting temperature, especially at higher pulse fluences. For this reason, pulse durations of less than about 10 ps will generate very small heat affected zones since heat conduction does not have a considerable effect on the energy dissipation during that short time period.

The ablation rates are limited by the saturation of the ablated volume per pulse when the pulse fluence is increased. The ablated volume per pulse is zero at the threshold fluence and increases with fluence but only logarithmically. At a fixed output power, more volume can therefore be ablated if the energy fluence is lowered, while simultaneously increasing the pulse repetition rate (Fig.1). As has been shown by Neuenschwander et al., 2012, the maximum ablation rate occurs at a pulse fluence of e^2 times the threshold fluence. (Fig. 2). The ablation rate, C (in mm^3/[W min]), is given by:

$$C = \frac{30\ \delta}{F} \left(ln \left[\frac{F}{F_{th}}\right] \right)^2 \tag{3}$$

where F is the average fluence in J/mm^2, F_{th} is the average threshold fluence, and δ is the energy penetration depth per pulse in mm. For a Gaussian beam that is focused to a spot diameter 2w, the average fluence is defined as $E/\pi w^2$, where E is the pulse energy. Typical values for the energy penetration depth per pulse δ are in the range of 10 to 100 nm for metals and semiconductors, and greater 300 nm for glasses. At the optimum fluence, with $F = e^2\ F_{th}$, the maximum ablation rate C_{max} is connected to the threshold fluence via:

$$C_{max} = \frac{120\ \delta}{F_{th}} \tag{4}$$

At the optimum fluence, the ablation depth per pulse and the ablated area are given by 2δ and πw^2, respectively.
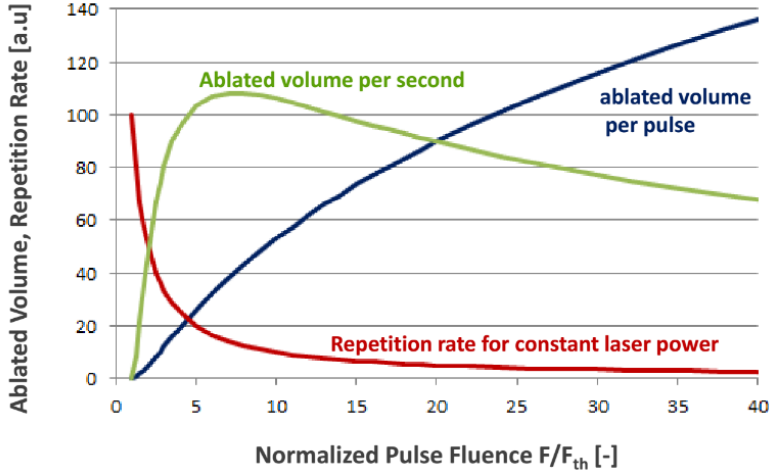
Fig.1. Ablated volume per pulse as a function of normalized pulse fluence and the corresponding dependence of the repetition rate on pulse fluence to maintain constant laser power. The ablated volume per second is the product of ablated volume per pulse and the repetition rate, and exhibits a maximum at a fluence of about 7.4 times the threshold fluence.

Instead of using the ablation rate C to characterize the process efficiency, a more practical figure of merit is the ablated volume per time, introduced here as R, in mm³/min. Since we want to compare lasers at different emission wavelengths, we can make a prediction for the process speed by assuming that the output power decreases proportionally to the wavelength. This assumption reflects the typical frequency conversion efficiencies, with the output powers in the green and UV being about 50 % and 33 % of the incident infrared power, respectively. By using Eq.4, the maximum process speed $R_{max}(\lambda)$, at the optimum fluence, as a function of laser wavelength λ then reads:

$$R_{max}(\lambda) = \frac{\lambda}{\lambda_0} R_{max}(\lambda_0) \frac{\delta(\lambda)\, F_{th}(\lambda_0)}{\delta(\lambda_0)\, F_{th}(\lambda)}$$

(5)

where λ_0 is the infrared wavelength (i.e. 1035 nm). We expect the process speed to linearly decrease with decreasing wavelengths. This is because the damage threshold fluence is, in a good approximation, proportional to the energy penetration depth, leading to the ratio on the right side of Eq.5 being around 1. We therefore expect the process speed at 517 nm and 345 nm to be only half and one-third, respectively, compared to the process speed at 1035 nm.

3. Experimental Set-up

We used a modelocked Yb-Fiber MOPA at 1035 nm with an output power of up to 40 W, repetition rates of 250 kHz and 500 kHz, a spectral bandwidth of 8 nm (FWHM) and stretched pulses at the laser exit of 600 ps duration (Fig. 2). The pulses were compressed using a double-pass, dual-grating compressor with variable length to access pulse durations between 400 fs and 18 ps. The compressed pulses were attenuated with a rotatable half-wave plate and a polarizer. A quarter-wave plate transformed the light into circular polarization before entering the scan head. External frequency conversion in LBO crystals, maximum output powers of 20 W at 517 nm and 6 W at 345 nm (at 500 kHz, before pulse stretching). In order to be able to

use UV pulse durations between 500 fs and 14 ps the pulses had to be stretched in the UV, after using 350 fs pulses to maximize the third harmonic generation efficiency. The UV pulse compression stage exhibited a UV power loss of about 40 %, due to the high losses of the UV transmission gratings (~ 20 % per grating pass, 2,450 lines/mm). At a repetition rate of 500 kHz, the maximum UV power entering the scanner was 2 W. All optics were AR-coated or HR coated at the wavelength being used for the ablation tests. At all three wavelengths, spot diameters in the range of 12 µm to 36 µm were generated at the work surface.

In order to accurately determine the ablation rates, rectangular cavities of 2-3 mm lengths and 0.3-0.5 mm width were ablated using a spot overlap of 60 % in both scanning directions (Fig. 3). This overlap was chosen after measuring the ablation rates for 9 different spot overlaps between 10 % and 90 % as a function of fluence and pulse duration for different materials. For a spot overlap of 60 % and higher, the maximum ablation rates were very similar. A lower pulse overlap of 60 % was chosen to avoid any possible melting of the ablated surface. The cavities were ablated to a depth of about 100 µm, which required up to 400 repetitions of the two-dimensional scan pattern. During the total ablation process, each spot on the rectangular area is hit by about 1,200 pulses. The ablation rate was calculated after measuring the ablation depth with a microscope, using only the central 300 µm square section of the ablated cavity.
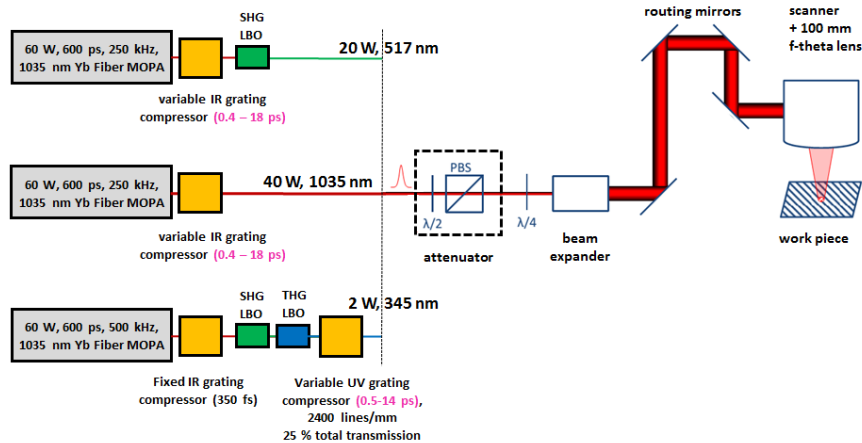

Fig.3. Experimental set-up for measuring ablation rates at three laser wavelengths as a function of pulse duration and pulse fluence. Beam routing and scan optics were AR-coated for the wavelength being used.
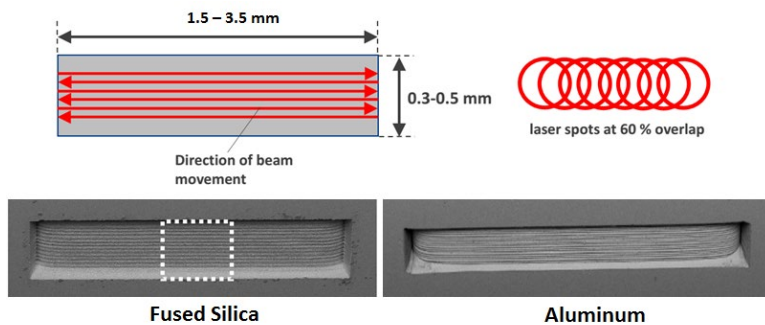

Fig.4. Scan geometry used for ablation with 60 % spot overlap in both directions. The photos show electron microscope images of two cavities in FS (1.5 mm long) and Al (3.5 mm long).

Since the optimum fluence is directly proportional to the threshold fluence, we measured ablation thresholds for various materials for single-shot and N=1,200 shots per location. The single-shot threshold measurements are depicted in Fig. 6. For N pulses per spot, the threshold fluence $F_{th}(N)$ will decrease due to incubation:

$$F_{th}(N) = F_{th}(1) \, N^{S-1} \tag{6}$$

where S is the incubation parameter. Incubation will lead to a decrease of the optimum fluence for ablation. We determined the incubation parameters to be 0.83 for FS, 0.69 for Sapphire, 0.75 for Cu, 0.76 for Au, 0.8 for Ni, and 0.85 for Al. It is interesting to note that the threshold fluences stay constant below a pulse duration of about 8 ps. For longer pulses, the heat conduction will increase the affected volume leading to the well-known threshold fluence scaling with the square-root of the pulse duration. This is in agreement with the Two-Temperature-Model which predicts constant damage thresholds below a characteristic pulse duration (Sherman, 1989). The characteristic pulse duration does not depend on the laser wavelength, since it is determined by the interaction of electrons and lattice rather than the interaction between photons and electrons.
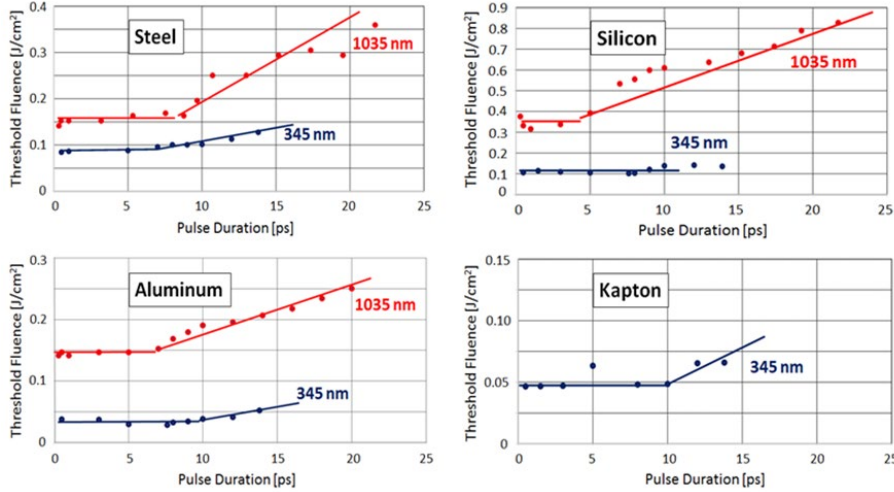

Fig. 5. Measured single-shot damage threshold fluence (average fluence) as a function of pulse duration at 1035 nm and at 345 nm. The spot diameter was 36 µm at 1035 nm, and 20 µm at 345 nm.

4. Measured Ablation Rates and Process Speeds

Figure 6 shows the measured ablation rates for various materials. Due to the page number limitation, we are only showing some representative metals, semiconductors, and dielectrics, and provide a summary of the maximally obtained ablation rates for the rest of the materials further below. In general, the measured ablation rates curve show the expected shape, with an optimum fluence at about 7.4 times the threshold fluence. We also measured the ablation depth per pulse at the optimum fluences (which at that fluence is equal to 2δ) by measuring the depth of the ablated cavities and dividing by the number of pulses that were used per location. We found that the measured ablation depths per pulse are in agreement with the values provided by Eq. 4, when the measured maximum ablation rates are inserted. For materials exhibiting free

electrons (e.g. metals, and semiconductors) and wavelengths of 1035 nm and 517 nm, the energy penetration depth δ increases as the pulse duration is increased with a typical increase by a factor 1.5 - 2 between 10 ps and 400 fs, leading to highest ablation rates for sub-ps pulses. At 345 nm, penetration depths were mostly independent of pulse duration. For glasses and crystals, ablation rates maximize for longer pulse duration in the 10 - 20 ps range. This is due to the lack of free electrons which leads to high threshold fluences and correspondingly high penetration depths. Operation at sub-ps pulse duration leads to break-down effects due to nonlinear interactions with the material, as can be clearly seen for ablation of BK7 at 1035 nm.

It is important to note that the optimum pulse fluences for all metals, semiconductors and plastic materials we measured were in the range of 0.5 – 1.5 J/cm^2. This poses a challenge for micro-processing since for a typical laser power of 50 – 100 W and a repetition rate of 500 kHz, the average pulse fluences on the material for a 20 μm spot diameter are in the range of 32 to 64 J/cm^2. Reaching the optimum fluence, therefore, requires either much larger spot diameters, or operating at 30-60 times higher repetition rates. One possible way to solve this problem is to use the ultrafast lasers in a burst mode, by using a burst of amplified seed laser pulses with 10s of ns separation while keeping the distance between bursts at the μs level. A summary of the measured maximum ablation rates and corresponding maximum process speeds is shown in Fig. 7 for selected materials.
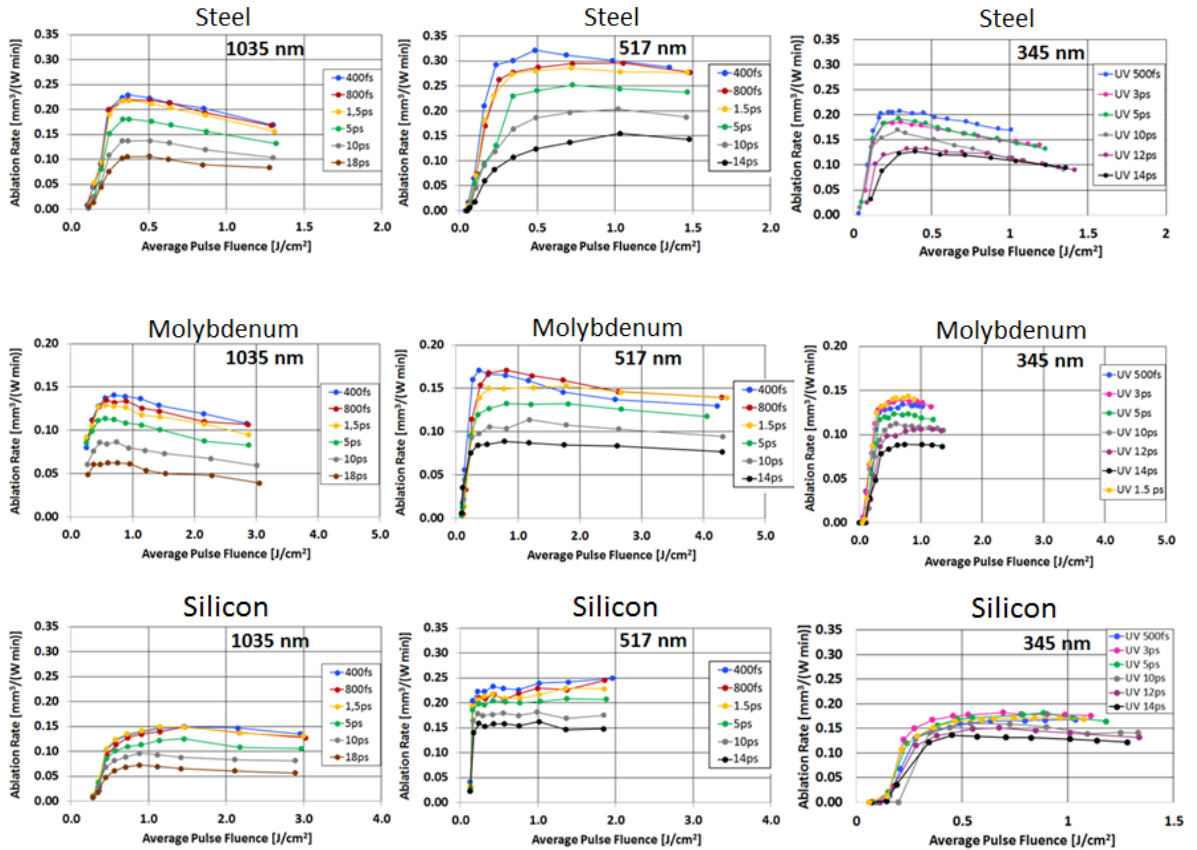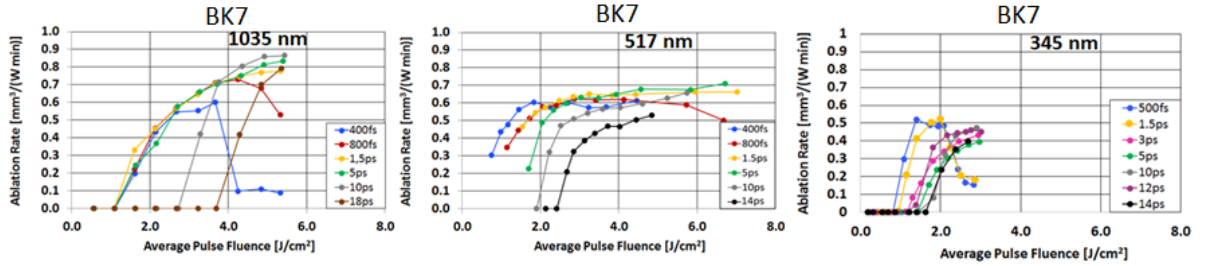
Fig.6. Measured ablation rates as a function of the pulse fluence for Steel, Molybdenum, silicon, and BK7 at 1035 nm, 517 nm and 345 nm. The curve parameter is the pulse duration. Spot Diameters: 25 µm at 1035 nm, 12 µm at 517 nm, and 20 µm at 345 nm. Repetition rate: 250 kHz at 1035 nm and 517 nm, and 500 kHz at 345 nm.

To calculate the process speeds, we assumed output powers of 100 W, 50 W and 30 W, at 1035 nm, 517 nm and 345 nm, respectively, which represents the state-of-the art of industrial ultrafast lasers in use. As expected from Eq. 5 in Chapter 1, the process speeds decrease with decreasing wavelength for most of the materials shown. However, there are exceptions, like Nitinol at 517 nm, and plastic materials that exhibit much higher process speeds for UV laser ablation due to a strong linear absorption, as shown in Fig. 8. Also the plastic materials exhibit very low optimum fluences of about 0.75 J/cm^2. Considering all materials investigated the general statement can be made that the decision to use a shorter wavelength is not driven by an increase the process speed, but rather, as we will be discussed below, by minimizing HAZ or surface roughness.
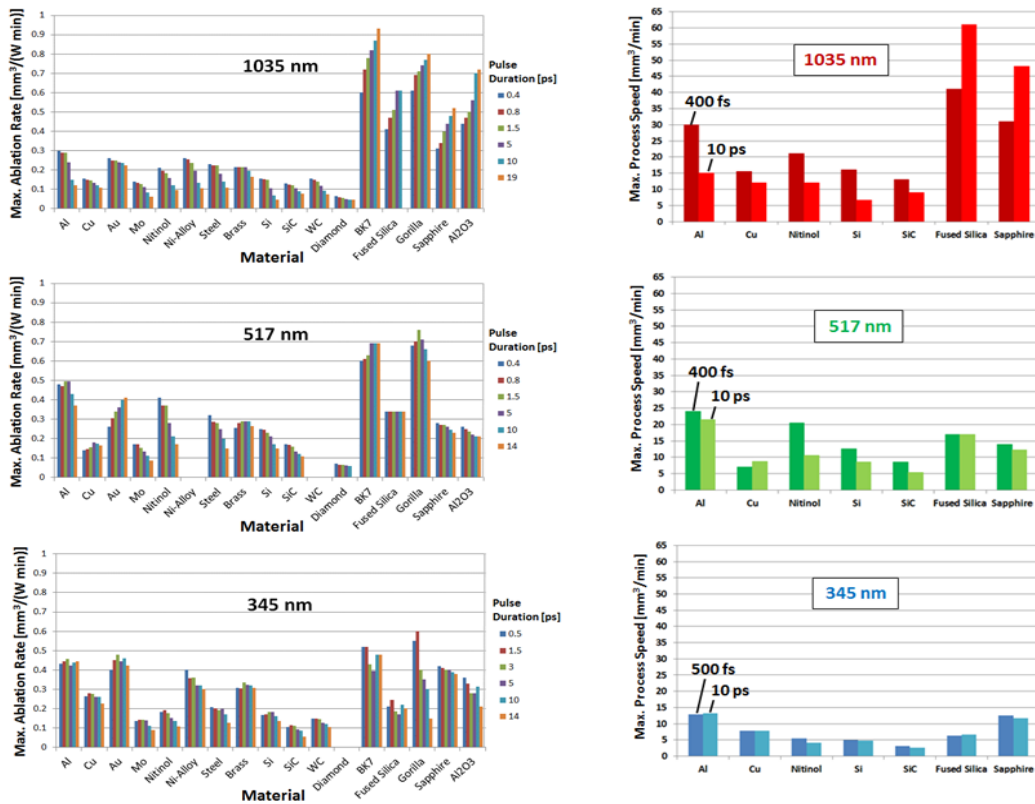
Fig.7. Measured maximum ablation rates (left) and corresponding maximum process speeds (right) for various materials. The parameter of the bars is the pulse duration, with the shortest pulse duration at the left. To calculate the process speeds, output powers of 100 W, 50 W and 30 W at 1035 nm, 517 nm, and 345 nm were assumed. For Gorilla glass and Al_2O_3 ceramic and pulse durations greater 1.5 ps, the maximum pulse fluences at 345 nm were not high enough to reach the ablation rate maximum. For these two materials, the highest measured rates are shown.
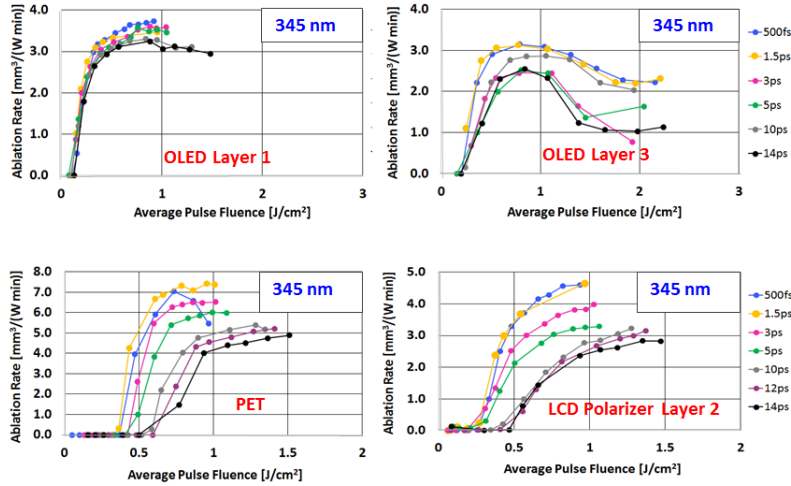

Fig.8. Measured ablation rates as a function of the average pulse fluence for different plastic materials at 345 nm. The curve parameter is the pulse duration. Spot Diameter: 20 µm for all materials, except for OLED Layer 3 (12 µm spot diameter). Repetition rate: 500 kHz.

5. Measured Heat Affected Zone

The fact that the damage threshold fluences are constant below about 8 ps leads us to expect that the width of the heat affected zone is also a constant over this range of pulse durations. We ablated lines in several materials as a function of fluence and pulse duration and measured the HAZ by visual inspection under a microscope. The lines were ablated with 150 passes, with a pause of 1 s between passes to avoid any melting effects. Figure 9 shows the measured width of the HAZ as a function of pulse duration for different fluences for Steel and Kapton. In general, the HAZ is independent of pulse duration when operating at the optimum fluence. As the fluence is increased the HAZ width increases and, in addition, a dependence on the pulse duration will materialize, with shorter pulses providing smaller HAZ. Operating at the optimum fluence of about 8 times the ablation threshold fluence will lead to maximum ablation rate and minimizes the HAZ, independent of pulse duration. This is actually not surprising, since a higher fraction of the energy is transferred into the ablation process instead of being dissipated into the material. The HAZ can be made even smaller for pulse fluences that are below the optimum one, but in this case the ablation rate is also much lower with a reduction of the width of the ablated line.

In addition, there is a linear dependence of HAZ width on the spot diameter of the laser beam as the example of Kapton in Fig. 9 clearly indicates. Using a shorter wavelength for ablation enables much smaller spot sizes during processing because the Rayleigh range at 345 nm is three times larger as compared to 1035 at the same spot diameter. This reduction in spot size is especially important for any plastics, as these materials are poor conductors leading to larger HAZ. While HAZ widths of around 6-8 µm are standard for metals for a 20 µm spot diameter, the heat affected zone in plastic materials like Kapton or PET can be up to ten times wider. Minimizing the spot diameter by selecting a UV laser wavelength is therefore essential for processing these heat-sensitive materials.
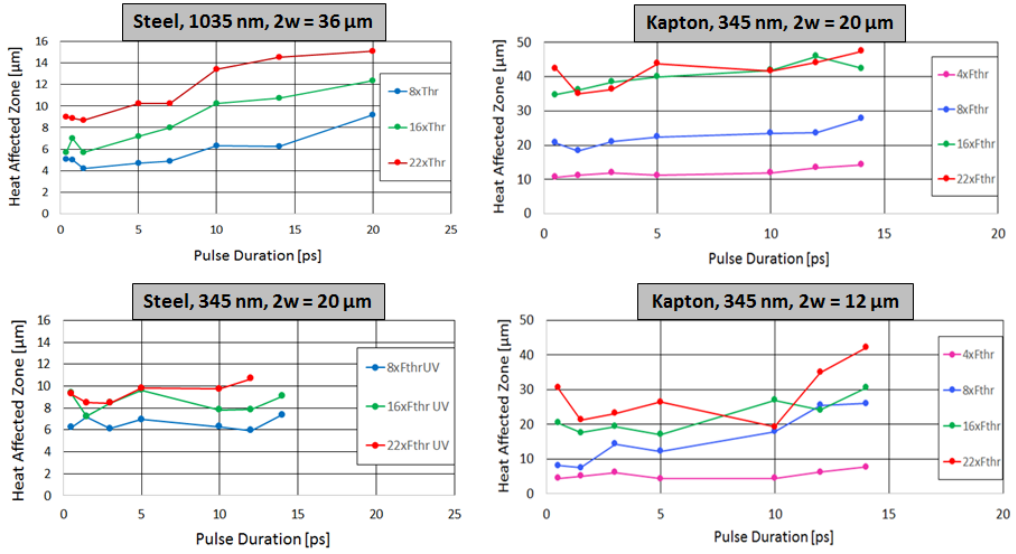
Fig. 9. Measured HAZ width of ablated lines as a function of the pulse duration for Steel at different laser wavelengths (left), and for Kapton at 345 nm for different spot diameters (right). Curve parameter is the pulse fluence relative to the ablation threshold fluence. Repetition rate of 200 kHz for Steel, and 500 kHz for Kapton. 60 % spot overlap. Optimum fluence for Kapton at 345 nm was 0.5 J/cm^2 for all pulse durations.

6. Summary and Conclusion

We have measured the ablation rates for 25 materials that are commonly used in industrial manufacturing as a function of pulse duration and pulse fluence for wavelengths of 1035 nm, 517 nm and 345 nm. Maximum ablation rates were in the range of 0.1-0.3 mm^3/(W min) for metals and semiconductors, up to 0.8 mm^3/(W min) for glasses, and up to 8 mm^3/(W min) for transparent plastic materials. The highest ablation rate was found for black rubber with 12 mm^3/(W min) at 1035 nm. Materials that were measured but not mentioned above, were FR4, PEEK, and diamond. For metals, semiconductors and plastics, the optimum average pulse fluences were in the range of 0.5 – 1.5 J/cm^2 for all three wavelengths and highest ablation rates were consistently at sup-ps pulse durations. For transparent glasses and crystals, maximum ablation rates were measured for pulse durations of 10 - 20 ps with optimum fluences of around 6 J/cm^2 at 1035 nm.

In order to ablate at these low pulse fluence levels, 100 W-class ultrafast lasers need to either be operated at repetition rates of around 10-20 MHz for typical spot diameters of 20-30 µm, or large spot sizes have to be used, which is certainly a possibility for large area applications, like surface-texturing. Most industrial applications for ultrafast lasers, however, are in cutting using an ablative process and they do require small spot diameters. In this case, operating the laser in burst mode, with delivering a group of 5-20 pulses with distance of tens of nanosecond may be the best solution to reach maximum ablation rates and minimizing the heat affected zone (Hodgson et al., 2019). In a realistic scenario, a laser could be operated at a repetition rate of 1 MHz, and increasing the number of pulses in a burst from initially 1 to 10 or 20, will not only increase the ablation rate, but will also lead to less thermal damage and a reduction in HAZ. This, however, will require careful optimization of the temporal distance between individual pulses in the burst, depending on the heat conduction of the material. While a pulse separation of 10-20 ns is long enough for

metals and semiconductors to allow cooling down of the ablated spot between pulses, plastics may need much longer pulse separation to avoid thermal effects.

References

Strategies Unlimited, Lasers & Photonics Marketplace Seminar, PennWell 2016.

Anisimov S.I., Kapeliovich, B.L., Perel'man, T.L., 1974. Electron emission from metal surfaces exposed to ultrashort laser pulses, Sov. Phys. JETP 39, p. 375.

Sherman, N.K., Brunei, F., Corkum, P.B., Hedmann, F.A., 1989. Transient response of metals to ultrashort pulse excitation, Opt. Eng. 28(10), p. 1114.

Qiu, T.Q., Tien, C.L., 1992. Short-pulse laser heating on metals, Int. J. Heat Mass Transfer 35(3), p. 719.

Nolte, S., Momma, C., Jacobs, H., Tünnermann, A., Chichkov, B.N., Wellegehausen, B., Welling, H., 1997. Ablation of metals by ultrashort laser pulses, J. Opt. Soc. Am. B14(10), P. 2716.

Breitling, D., Ruf, A., Dausinger, F., 2004. Fundamental aspects in machining of metals with short and ultrashort laser pulses, Proc. SPIE vol. 5339, p. 49.

Neuenschwander, B., Jaeggi, B., Schmid, M., Rouffiange, V., Martin, P.-E., 2012, Optimization of the volume ablation rate for metals at different laser pulse-durations from ps to fs, Proc. SPIE vol. 8243, p. 824307.

Neuenschwander, B., Jaeggi, B., Schmid, M., 2012. From ps to fs: dependence of the material removal rate and the surface quality on the pulse duration for metals, semiconductors and oxides. In: ICALEO 31, paper M1004, Anaheim, CA 2012.

Wellershoff S.-S., Hohlfeld, J., Güdde, J. Matthias, E., 1999. The role of electron-phonon coupling in femtosecond laser damage of, Appl. Phys. A 69, p. 99.

Hodgson, N., Laha, M. , Lee, Tony S., Steinkopff, A., Heming, S., 2019. Industrial femtosecond lasers and material processing. In: Industrial Laser Solutions, PennWell Publishing, January 22, 2019.